Magnesium Technology 2013
Edited by: Norbert Hort, Suveen N. Mathaudhu, Neale R. Neelameggham, and Martyn Alderman
TMS (The Minerals, Metals & Materials Society), 2013

Mathematical Modeling of the Effect of Roll Diameter on the Thermo-Mechanical Behavior of Twin Roll Cast AZ31 Magnesium Alloy Strips

Amir Hadadzadeh[1], Mary Wells[1]
1. Mechanical and Mechatronics Engineering Department, University of Waterloo, Waterloo, ON, Canada

Keywords: Twin Roll Casting, Mathematical Modeling, AZ31 Magnesium Alloy, Roll Diameter.

Abstract

Although the Twin Roll Casting (TRC) process has been used in the aluminum sheet production industry for more than 60 years, the usage of this process to fabricate magnesium sheets is still at its early stages. Similar to other manufacturing processes, the development of the TRC process for magnesium alloys has followed a typical route of preliminary studies using a laboratory-scale facility, followed by pilot-scale testing and most recently attempting to use an industrial-scale twin roll caster. A powerful tool to understand and quantify the trends of the processing conditions and effects of scaling up from a laboratory size TRC machine to an industrial scale one is develop a mathematical model of the process. This can elucidate the coupled fluid-thermo-mechanical behavior of the cast strip during the solidification and then deformation stages of the process. In the present study a Thermal-Fluid-Stress model has been developed for TRC of AZ31 magnesium alloy for three roll diameters by employing the FEM commercial package ALSIM. The roll diameters were chosen as 355mm, 600mm and 1150mm. The effect of casting speed for each diameter was studied in terms of fluid flow, thermal history and stress-strain evolution in the cast strip in the roll bite region.

1- Introduction

Magnesium is a desirable material in the automotive industry since it is 33% lighter than aluminum and 70% lighter than steel. Currently, most of the magnesium usage in this industry is limited to die casting and a small portion is allocated to sheets. The reason for this is that the HCP structure of magnesium makes it very costly to produce wrought sheet products. One alternative for magnesium sheet production is twin roll casting (TRC) process which incorporates both casting and hot rolling in one process and consequently reduces the cost and energy consumption [1]. In the TRC process, the molten material is fed into the roll bite region from the entry side and from the exit side solid sheet material is obtained. This process has the capability of producing sheet with thicknesses between 2-10mm and typically experiences cooling rates in the range of 10^2-10^3°C/s during solidification [2]. This unique cooling condition leads to unique microstructure evolution during magnesium TRC.

Similar to all other manufacturing process development, the evolution of TRC for magnesium has started running preliminary trials for a number of alloys using a laboratory scale caster. This has then been followed by TRC casting at a pilot scale level and most recently following this success, the design of an industrial scale TRC caster for magnesium. A powerful tool to predict and analyze processing differences from laboratory to industrial casters is to mathematically model the process.

In the current study three roll diameters for magnesium TRC has been considered to study the changes in process history experienced by the sheet as you move from laboratory to industrial scale TRC. The laboratory scale caster is based on the one running at the Natural Resources Canada Government Materials Laboratory, CanmetMATERIALS located in Hamilton, Ontario, Canada with the roll diameter of 355mm. The pilot and industrial scales have been considered as roll diameters of 600mm and 1150mm, respectively. A 2D FEM thermal-fluid-stress mathematical model was developed previously with the commercial package ALSIM [3, 4] to simulate the thermo-mechanical behavior of the AZ31 magnesium alloy during TRC. This model has been extended to include the effect of roll diameter on the predicted results. The results are presented in this work.

2- Model Development

Figure 1 illustrates the schematic of the TRC process. The mathematical model includes heat transfer and fluid flow in the liquid metal, heat transfer, fluid flow and latent heat of fusion release in the mushy zone and deformation in the material once the coherency point is reached, heat transfer and plastic deformation in the solid phase, heat transfer from the magnesium sheet to the roll surface, and heat transfer inside the roll material and from the roll's sleeve to the circulated water.

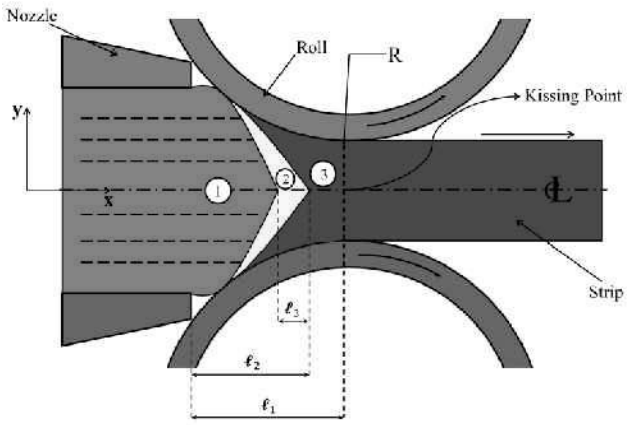

Figure 1- Schematic of the TRC process, region 1 is the liquid metal, region 2 is the mushy zone and region 3 is the solid strip, ℓ_1 is set-back distance, ℓ_2 is the solidification front position and ℓ_3 is the mushy zone depth.

The transport phenomena are considered as the conservation laws of mass, momentum and energy and shown by the general transport equation using Equation 1.

$$\frac{\partial}{\partial x_i}(\rho u_i C_\Phi \Phi) = \frac{\partial}{\partial x_i}\left(\Gamma_\Phi \frac{\partial \Phi}{\partial x_i}\right) + S_\Phi \quad (1)$$

where C_Φ is the coefficient of convection, Φ is the thermal-fluid variable, Γ_Φ is the coefficient of diffusion, S_Φ is source term, ρ is density (in kg/m^3) and u_i is velocity (in m/s).

The effects of latent heat of fusion release and fluid flow dump in the mushy zone are included by adding appropriate source terms [5].

For the thermal elastic-plastic model, the material is defined as an isotropic elastic-viscoplastic material. The velocity field below the coherency temperature which is used to calculate the strain is determined by minimizing the energy functional as shown in Equation 2.

$$\delta\pi = \int_\Omega \delta\boldsymbol{\varepsilon}^* . \boldsymbol{\sigma} d\Omega - \int_\Omega \delta\mathbf{u}^* . \rho\mathbf{g} d\Omega - \int_\Gamma \delta\mathbf{u}^* . \mathbf{t} d\Gamma = 0 \quad (2)$$

where π is functional, $\boldsymbol{\varepsilon}$ is the strain vector, $\boldsymbol{\sigma}$ is the stress tensor (in Pa), $\mathbf{u}$ is a displacement vector, $\mathbf{g}$ is the gravity vector (in m/s^2), $\boldsymbol{t}$ is the force per unit length (in N/m), Ω is the solution domain and Γ is the solution boundary.

The total strain imposed to the material is subdivided into thermal, elastic and viscoplastic components [6], and the constitutive equation shows the plastic behavior of material below the coherency temperature is defined as Equation 3 [6].

$$\boldsymbol{\sigma} = K(T).(\dot{\boldsymbol{\varepsilon}}_P + \dot{\varepsilon}_{Po})^{m(T)}(\boldsymbol{\varepsilon}_P + \varepsilon_{Po})^{n(T)} \quad (3)$$

where $\dot{\boldsymbol{\varepsilon}}_P$ is the plastic strain rate in s^{-1}, $\boldsymbol{\varepsilon}_P$ is the plastic strain, K is strength coefficient, n is the strain hardening exponent and m is the strain rate sensitivity exponent. $\dot{\varepsilon}_{Po}$ and ε_{Po} are small numerical constants needed to ensure that at a plastic strain of zero, the yield stress of the material is correct. For AZ31 a coherency temperature of 595°C (0.9 f_s) was assumed.

The commercial FE package, ALSIM, was used to develop the model and solve the above-mentioned equations to simulate the TRC process for AZ31 magnesium alloy. The thermo-physical and constitutive material properties were taken from the literature [7]. Appropriate boundary conditions were applied and the HTC was chosen equal to 11kW/m^2°C based on previous work [3, 4]. Table 1 shows the range of casting conditions used in the model. The casting temperature for all cases was 677°C, the entry height of the nozzle and the strip final thickness were considered identical as 12mm and 6mm, respectively, to keep the nominal reduction constant (50%), but since the set-back distance (distance between the nozzle entry and the kissing point, Figure 1) is affected by both reduction and roll diameter (as shown in Equation 4), three different set-back distances were obtained.

$$SB = l_1 = \sqrt{R\Delta h - 0.25\Delta h^2} \quad (4)$$

where R is the roll radius (in mm) and Δh is the reduction (the difference between entry and exit thickness) (in mm).

Table 1- Casting conditions modeled in the present study

Caster Set-Up	Roll Diameter (D) (mm)	Set-Back Distance (SB) (mm)	Strip Width (mm)	Casting Speed (v) (m/min)
Φ355mm	355	32.5	250	1.0-6.0
Φ600mm	600	42.3	600	
Φ1150mm	1150	58.7	1150	

3- Results and Discussions

3-1-Thermal History of the Strip

An acceptable casting speed (v) is determined by the temperature of the strip at the center-line at the exit point of the caster; it should be less than solidus temperature. Otherwise, a non-fully solidified strip exits the caster and severe defects such as a breakout of liquid metal from the sheet can occur. The model-predicted temperature profiles for various casting conditions suggest that the maximum achievable casting speeds for Φ355mm, Φ600mm and Φ1150mm are 2.5m/min, 3.0m/min and 5.0m/min, respectively. Bigger roll diameters (D) provides a longer arc of contact between strip and roll surface and consequently more heat transfer from the cast material to the roll material occurs leading to a lower temperature at the exit point.

Figure 2 illustrates the model-predicted solidification contour map for various set-ups and casting speeds using a normalized set-back distance. As expected, increasing the casting speed reduces the heat extracted from the strip and leads to higher exit temperatures. As more heat is extracted from the strip and it solidifies earlier in the roll bits, more plastic deformation is experienced by the cast material. As expected the evolution of the solid shell and its thickness is also affected by the TRC casting parameters. Figure 3 shows the model-predicted solid shell thickness development on the roll surface and how it is affected by the roll diameter and casting speed.

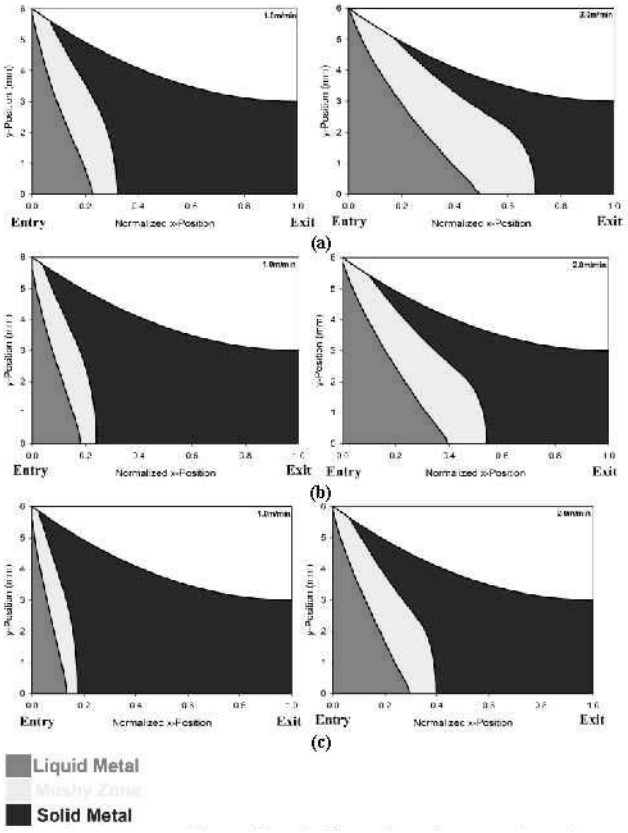

Figure 2- Model-predicted effect of casting speed on the solidification profile for a) Φ355mm, b) Φ600mm and c) Φ1150mm.

Referring to Figure 3, casting with higher speed, causes the solid shell develop on a longer distance. This also leads to formation of a thinner shell through the roll bite. Moreover, increasing the roll diameter leads to accomplishment of solidification on a shorter distance and a thicker solid layer appears on the roll surface.

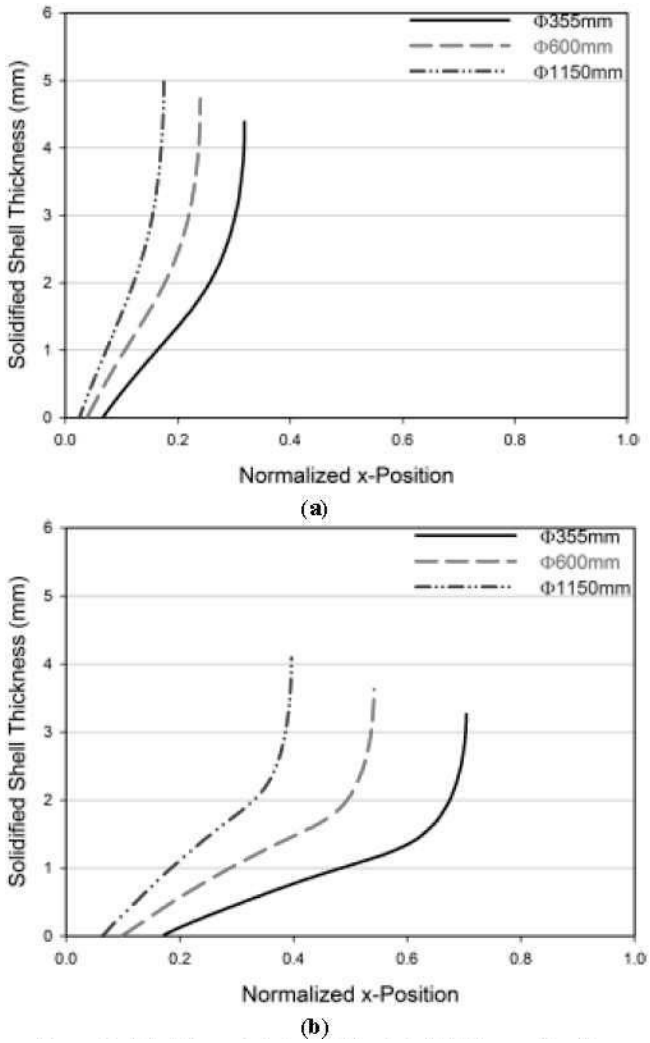

Figure 3- Model-predicted solidified shell thickness for a) v=1.0m/min and b) v=2.0m/min.

Figure 4 shows the model-predicted effect of casting speed and roll diameter on the mushy zone depth at the center-line for casting speed ranges between 1.0-2.5m/min. As observed, increasing the casting speed and decreasing the roll diameter cause a deeper mushy zone. The impact of roll diameter is more pronounced at higher casting speeds. Mushy zone depth is important since center-line segregation formation is directly related to this parameter.

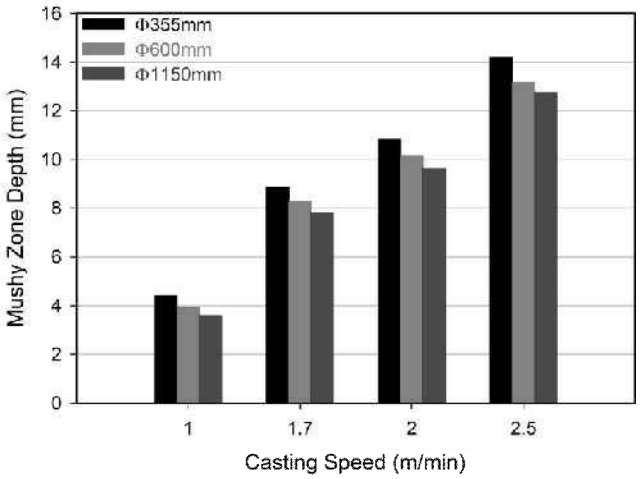

Figure 4- Model-predicted mushy zone depth (ℓ_3) affected by roll diameter and casting speed.

3-2-Mechanical Behavior of the Strip

Figure 5 illustrates the normal (yy-component) and shear stress development on the strip surface during AZ31 TRC. The relative motion between roll and strip leads to the unique shape of the shear stress graph. This relative motion at the strip/roll interface leads to positive, zero and negative shear stress prior, at and beyond the neutral point, respectively. The peak of yy-stress also occurs at the neutral point.

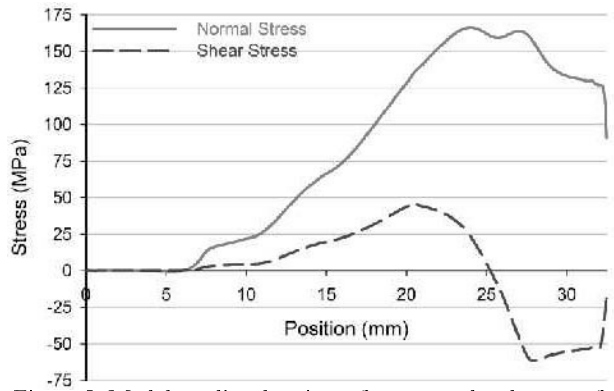

Figure 5- Model-predicted strip surface stress development for Φ355mm at v=1.0m/min.

The model-predicted effect of roll diameter on the surface normal stress is shown in Figure 6 on a normalized x-axis. As mentioned previously, by scaling up the caster the amount of solid material in the roll bite region which experiences plastic deformation increases which leads to development of higher level of normal stress on the strip surface. Figure 7 represents the corresponding shear stresses. As observed, the neutral point does not shift significantly relative to the entry position by increasing the roll diameter.

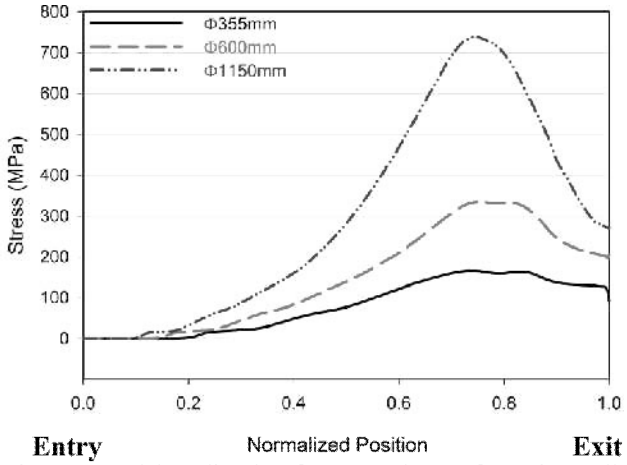

Figure 6- Model-predicted surface normal stress for various roll diameters at v=1.0m/min.

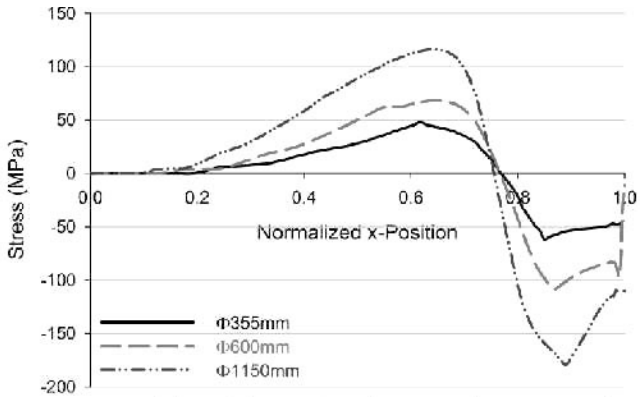

Figure 7- Model-predicted surface shear stress for various roll diameters at v=1.0m/min.

Figure 8 shows the model-predicted effective strain at the center-line at v=1.0m/min for the three roll diameters. The effective strain represents the amount of plastic deformation experienced by the cast material during the hot deformation stage of TRC. The strain development begins immediately at the point where the mushy material reaches the coherency temperature. A sharp jump to a plateau is observed prior the full solidification; this is due to a high strain rate experienced by the material in this region. Beyond the solidus temperature, the effective strain continues to increase gradually up to the maximum value and no change is observed after the neutral point since the material is not deformed beyond this point. For all cases, the maximum effective strain will be less than 0.5, since the nominal reduction of all cases studied is 50%. As observed in Figure 8, the amount of effective strain at the exit point increases by scaling up the caster. However, the rise of the effective strain is not as significant as the surface normal stress.

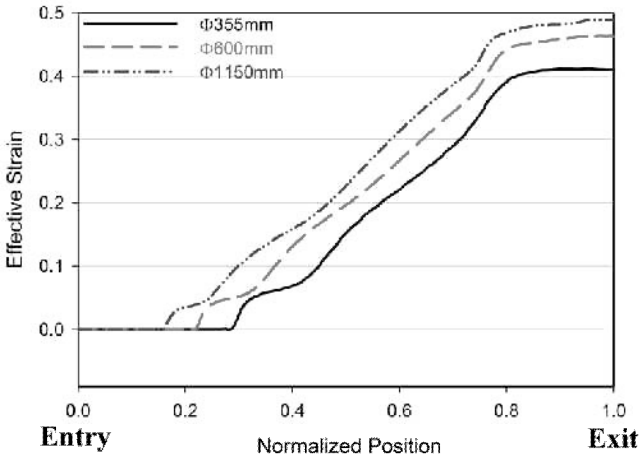

Figure 8- Model-predicted effective strain at center-line at v=1.0m/min.

The relationship between the maximum effective strain at center-line at exit point of the caster ($\varepsilon_{eff\text{-}max}$) and casting speed ($v$) is shown in Figure 9 for different set-ups. As seen the relationship is linear and the effect of roll diameter on the strain is more pronounced at higher casting speeds. For low casting speeds, since the amount of solid material increases inside the roll bite region and hot deformation starts at points closer to the nozzle entry, the effective strain approaches 0.5 for all roll diameters. Table 2 shows the linear $\varepsilon_{eff\text{-}max}$-$v$ relationship for each set-up.

Table 2- Effective strain-casting speed relationship

Caster Set-Up	Relationship
Φ355mm	$\varepsilon_{eff-max} = -0.2468v + 0.6449$
Φ600mm	$\varepsilon_{eff-max} = -0.1976v + 0.6476$
Φ1150mm	$\varepsilon_{eff-max} = -0.1226v + 0.5885$

Integrating the effect of both casting speed and roll diameter together is helpful in terms of predicting the maximum effective strain at the center-line at the exit point for a caster set-up in the range of roll diameter 355mm to 1150mm. Figure 10 illustrates such integration as a contour map. As expected, more plastic deformation is obtained at lower casting speeds and bigger roll diameters.

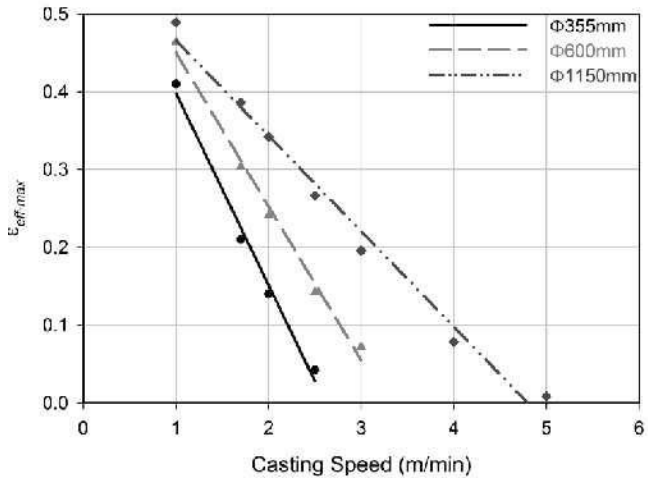

Figure 9- Model-predicted relationship between $\varepsilon_{eff\text{-}max}$ and v.

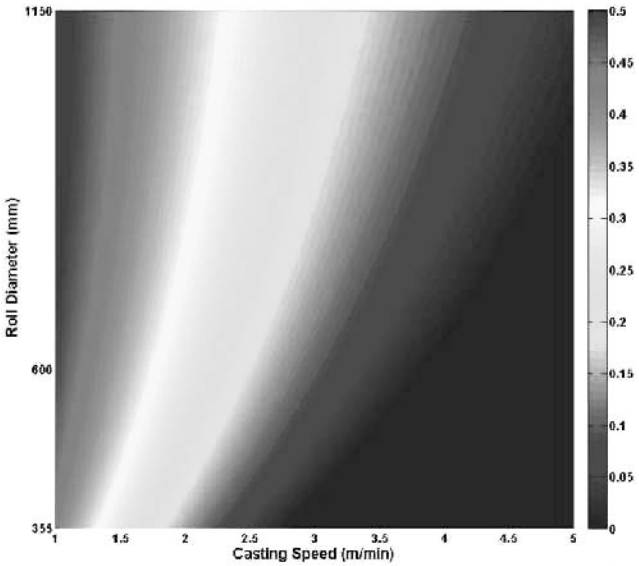

Figure 10- Model-predicted contour map of the effect of roll diameter and casting speed on the centre-line effective strain in the strip.

4- Conclusions

In the current study a 2D FEM thermal-fluid-stress model was employed to study the effect of roll diameter on the thermo-mechanical behavior of AZ31 during Twin Roll Casting. The results showed that by increasing the roll diameter, higher casting speeds are achievable. Scaling up the caster leads to formation of a thinner mushy zone at center-line which then decreases the risk of center line segregation formation.

The level of normal stress on the strip surface increases by scaling up the caster; however, the neutral point position does not shift significantly.

By increasing the roll diameter, the amount of plastic deformation experienced by the solid material increases; this parameter is shown by the maximum effective strain at the center-line at the exit point of the caster ($\varepsilon_{eff\text{-}max}$). The relationship between $\varepsilon_{eff\text{-}max}$ and casting speed is linear for each set-up.

Acknowledgments

This work was done as part of the Canadian NSERC Strategic Magnesium Network (MagNET) and the authors gratefully acknowledge funding received for this work.

References

[1] D. Liang, C. B. Cowley, *"The Twin-Roll Strip Casting of Magnesium"*, Journal of the Minerals, Metals and Materials Society, 56 (5) (2004), 26-28.

[2] H. S. Di, Y. L. Li, Z. L. Ning, Z. Li, X. Liu, G. D. Wang, *"New Processing Technology of Twin Roll Strip Casting of AZ31B Magnesium Strip"*, Materials Science Forum, 488-489 (2005), 615-618.

[3] A. Hadadzadeh, M. A. Wells, E. Essadiqi, *"Mathematical Modeling of the Twin Roll Casting Process for AZ31 Magnesium Alloy – Effect of Set-Back Distance"*, Magnesium Technology 2012, [ed.] S. N. Mathaudha, W. H. Sillekens, N. R. Neelameggham and N. Hort, TMS 141st Annual Meeting and Exhibition, Orlando, FL, 2012, pp. 141-144.

[4] A. Hadadzadeh, M. A. Wells, E. Essadiqi, *"Mathematical Modeling of the Twin Roll Casting Process for AZ31 Magnesium Alloy – Effect of Strip Thickness"*, Proceedings of 9th International Conference on Magnesium Alloys and their Applications, [ed.] W. J. Pool and K. U. Kainer, Vancouver, Canada, 2012, pp. 177-182.

[5] J. Zeng, R. Koitzsch, H. Pfeifer, B. Friedrich, *"Numerical Simulation of the Twin-Roll Casting Process of Magnesium Alloy Strip"*, Journal of Materials Processing Technology, 209 (2009) 2321-2328.

[6] M. M'Hamdi, A. Mo, H.G. Fjær, *"TearSim: A Two-Phase Model Addressing Hot Tearing Formation During Aluminium Direct Chill Casting"*, Metallurgical and Materials Transactions A, 37A (2006) 3069-3083.

[7] B. J. Howes, M. A. Wells, R. Bathla, D. M. Maijer, *"Constitutive Behaviour of As-Cast Magnesium Alloy AZ31 Under Deformation Conditions Relevant to DC Casting"*, Proceedings of the 2nd International Light Metals Technology Conference, [ed.] H. Kaufmann. St. Wolfgang, Austria, 2005.